G41B-0688 HIGH-PERFORMANCE SYSTEM FOR MONITORING GROUND DEFORMATION FROM RCM SAR DATA

Sergey V. Samsonov, Canada Centre for Mapping and Earth Observation, Natural Resources Canada, Ottawa, Ontario, Canada, Email: sergey.samsonov@canada.ca

ABSTRACT

Differential Interferometric Synthetic Aperture Radar (DInSAR) based mapping of surface deformation has proven valuable in a variety of geoscience applications. Conventional approaches to DInSAR analysis require significant expertise and are not suited to addressing the opportunities and challenges presented by the large multi-temporal SAR datasets generated by future radar constellations. As a result, the Canada Centre for Mapping and Earth Observation (CCMEO) developed, in support of Natural Resources Canada and Government of Canada priorities, a system for automatic generation of standard and advanced deformation products based on DInSAR technology from RADARSAT Constellation Mission (RCM) Synthetic Aperture Radar (SAR) data. Existing RADARSAT-2 processing algorithms were adapted to RCM specifications and novel advanced processing algorithms were developed to address the large data sets resulting from the constellation's four-day rapid revisit cycle. This permitted expanding the DInSAR functionality across a wide-range of spatial and temporal scales. The system architecture is scalable and can be expanded to serve a large number of clients; it can simultaneously address multiple application areas including natural and anthropogenic hazards, natural resource development, permafrost and glacier monitoring, coastal and environmental change and wetlands mapping.

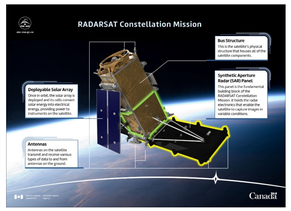

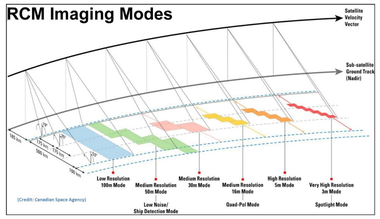

RCM launch date

February 2019

Table 1: RCM beam modes, where L is the slant range and azimuth spatial sampling, θ is the nominal incidence angle range, R and A are multi-looking numbers in range and azimuth respectively, and NESZ is the nominal Noise Equivalent Sigma Zero that describes the sensitivity of the SAR system.

Beam Name	Beam	Resolution (m)	Swath (Km)	Looks (R x A)	L (m)	θ°	NESZ (dB)
Ship Detection	ScanSAR	variable	350	5 x 1	1.4 x 34.4	40 - 58	variable
Low Noise	ScanSAR	100	350	4 x 2	8.7 x 69.1	19 - 58	-25
Low Resolution 100m	ScanSAR	100	500	8 x 1	4.2 x 69.1	19 - 54	-22
Medium Resolution 50m	ScanSAR	50	350	4 x 1	4.2 x 34.5	19 - 58	-22
Medium Resolution 30m	ScanSAR	30	125	2 x 2	4.2 x 23.0	19 - 47	-24
Medium Resolution 16m	Strip-map	16	30	1 x 4	6.3 x 2.2	19 - 47	-25
Quad-Polarization	Strip-map	9	20	1 x 1	3.1 x 2.9	24 - 44	-24
High Resolution 5m	Strip-map	5	30	1 x 1	2.1 x 2.2	19 - 54	-19
Very High Resolution 3m	Strip-map	3	20	1 x 1	1.4 x 1.9	19 - 54	-17
Spotlight	Spotlight	3 x 1	20 x 5	1 x 1	1.4 x 0.5	19 - 47	-17

Table 2: Supported applications.

Applications	Duration	Displacement Magnitude	DInSAR	SBAS-DInSAR	Offset-tracking	MAI	RSLC	RMLI	Coherence
Earthquakes	Abrupt	Small to very large	x		x	x			
Volcanoes	Gradual and abrupt	Small to very large	x	x					
Landslides	Gradual and abrupt	Small to very large	x	x					
Inter-seismic tectonics	Gradual	Predominantly small	x	x					
Permafrost	Gradual	Predominantly small		x					
Glacial motion	Gradual	Predominantly very large	x		x	x			
Anthropogenic (mining, groundwater, carbon capture and storage-CCS)	Gradual and abrupt	Predominantly small	x	x					
Change detection	Gradual and abrupt	N/A (Coherence and intensity only)					x	x	x

Table 3: Supported products.

Product	Description	Format	Unit
Footprint	Image footprint for displaying in Google Earth	kmz	
Digital elevation model (DEM)	Digital Elevation Model extracted from the source specified through EODMS interface	Float	m
Multi-looked intensity (RMLI)	Coregistered intensity images	Float	dB
Unfiltered coherence	Cross-correlation coefficient of the SAR image pair estimated over a small window	Float	
Filtered coherence	Unfiltered coherence after applying adaptive filtering	Float	
Wrapped unfiltered phase	Differential interferogram of the SAR image pair, flattened and topographic phase removed	Float	rad
Wrapped filtered phase	Differential interferogram after applying adaptive filtering	Float	rad
Unwrapped filtered phase	Unwrapped filtered differential interferogram	Float	rad
Displacement (DInSAR)	Ground displacement along the satellite line of sight (LOS)	Float	m
Multi-temporal displacements (SBAS DInSAR)	Time series of ground displacements for each SLC epoch	Float	m
Offset-tracking	Range and azimuth offset maps	Float	m
Multi-aperture interferometry (MAI)	MAI differential interferogram	Float	m

ACKNOWLEDGEMENT

The Canadian Space Agency (CSA) provided RADARSAT-2 data and funded the research project "The Development and delivery of on-demand RADARSAT Constellation mission ground deformation products based on advanced InSAR technology" under Data Utilization and Application Plan program. Figures were plotted with GMT and GNUPLOT software and statistical analysis was performed with R software.

Subsidence in Mexico City


http://hydrosphere6.weebly.com

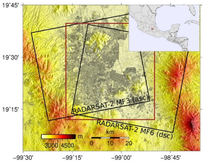

InSAR set	Time span	Resolution, m	$\theta°$	$\phi°$	N	M
R2-MF3 (asc)	20080730-20101211	3.1 - 4.6	349	43	30	117
R2-MF6 (dsc)	20081029-20110616	3.1 - 4.6	-170	49	30	147
Total:	20081029-20101211				58	264

Subsidence in Mexico City

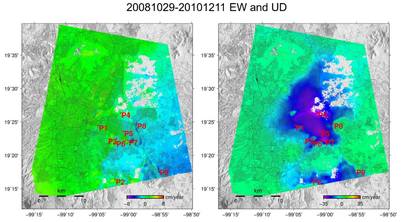

SCHEMATICS OF THE PROCESSING SYSTEM

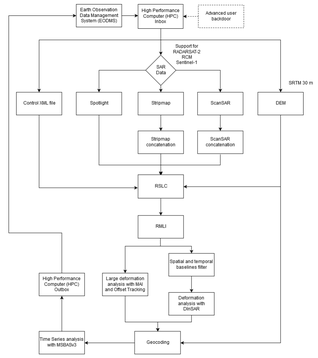

ABOUT THE PROCESSING SYSTEM

- Supports processing of RADARSAT-2, RCM and Sentinel-1 data;
- Based on GAMMA Remote Sensing software controlled with BASH scripts;
- Time series analysis is performed with the Multidimensional Small Baseline Subset (MSBASv3) software written in C++;
- Runs on a high performance computer (HPC) Linux cluster with over 2000 cores;
- Graphical user interface (GUI) is integrated into the Earth Observation Data Management System (EODMS);
- Processing is parallelized: SAR images and DInSAR interferograms are processed in parallel (sort of MPI), sub-processes are parallelized with OpenMP;
- Output products are produced in geotiff format;
- The system is accessible to the Government of Canada employees only, accounting information is managed by EODMS system;
- Real time processing is not guaranteed but an estimated latency is only a few hours.

EXAMPLES OF PRODUCTS PRODUCED BY THE SYSTEM FROM RADARSAT-2 DATA

Piton de la Fournaise Volcanic eruption and landslide

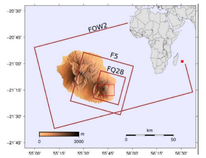

InSAR set	Time span	$\theta°$	$\phi°$	N	M
R2-FOW2 (asc)	20120321-20160402	346	36	30	162
R2-F5 (dsc)	20110908-20160414	-165	47	27	118
R2-FQ28 (dsc)	20140519-20150701	-165	47	9	33
Total:	20120211-20160402			64	313

Cerro Prieto Geothermal Field and 2010 M7.2 El Mayor-Cucapah


http://solarenergyfactsblog.com

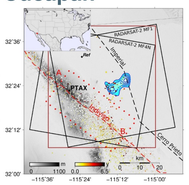

DInSAR set	Orbit	UTM	Coverage	$\theta°$	$\phi°$	N	M
RADARSAT-2, MF1	asc	01:43	20110913-20160724	349.4	38.4	53	434
RADARSAT-2, MF4N	dsc	13:36	20111001-20160811	-170.3	44.0	58	344
Total:			20111001-20160724			109	778

Piton de la Fournaise Volcanic eruption and landslide

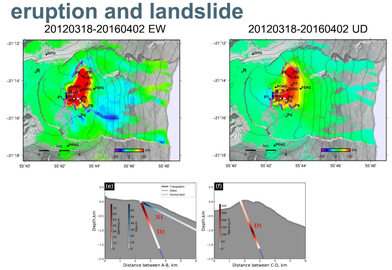

Cerro Prieto Geothermal Field and 2010 M7.2 El Mayor-Cucapah

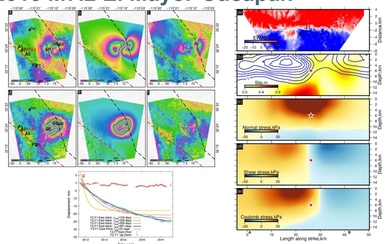

Campi Flegrei volcano

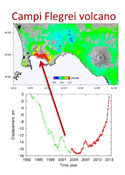

Alberta Oil sands

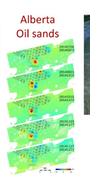

Urban subsidence in Vancouver

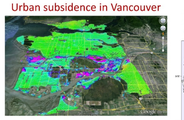

Haida Gwaii earthquake

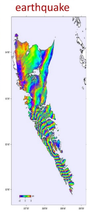

Pingo in NWT

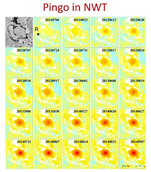

Saskatchewan potash mine

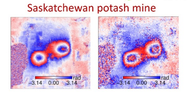

Subsidence in downtown Seattle

State Says Dewatering at Least Partially Caused Ground Settlement Near Bertha's Rescue Pit; Drilling Restart Delayed

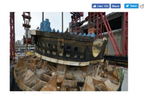

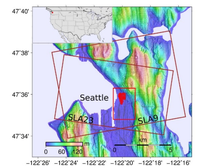

Table 1: DInSAR data sets used in this study: RADARSAT-2 Spotlight 9 and 23 (SLA9, SLA23); time span (in YYYYMMDD format), range-azimuth resolution, azimuth θ and incidence ϕ angles, number of available SAR images N, and number of calculated interferograms M for each data set.

DInSAR set	Time span	Resolution, m	$\theta°$	$\phi°$	N	M
R2-SLA9 (asc)	20120606-20150816	1.6 - 0.8	349	37	49	549
R2-SLA23 (dsc)	20120606-20150816	1.6 - 0.8	-172	47	46	539
Total:	20120606-20150816				50	1088

The 28 Sept, 2018 M7.5 Indonesia earthquake (RADARSAT-2 offset tracking)

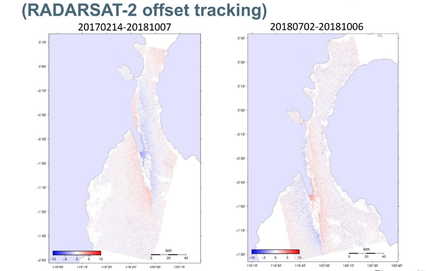

Subsidence in downtown Seattle

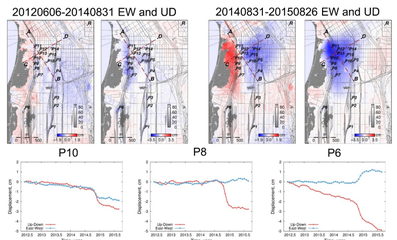

REFERENCES

1. Samsonov, S., d'Oreye, N., González, P., Tiampo, K., Ertolahti, L., and Clague, J. 2014. "Rapidly accelerating subsidence in the Greater Vancouver region from two decades of ERSENVISAT-RADARSAT-2 DInSAR measurements." Remote Sensing of Environment, Vol. 143(No. 5): pp. 180–191. doi: 10.1016/j.rse.2013.12.017.
2. Samsonov, S., Gonzalez, P., Tiampo, K., and d'Oreye, N. 2014. "Modeling of fast ground subsidence observed in southern Saskatchewan (Canada) during 2008–2011." Natural Hazards and Earth System Sciences, Vol. 14: pp. 247–257. doi: 10.5194/nhess-14-247-2014.
3. Samsonov, S.V., Tiampo, K.F., Camacho, A.G., Fernández, J., and González, P.J. 2014. "Spatiotemporal analysis and interpretation of 1993–2013 ground deformation at Campi Flegrei, Italy, observed by advanced DInSAR." Geophysical Research Letters, Vol. 41(No. 17): pp. 6101–6108. doi: 10.1002/2014GL060595.
4. Samsonov, S., Czarnogorska, M., and White, D. 2015. "Satellite interferometry for high-precision detection of ground deformation at a carbon dioxide storage site." International Journal of Greenhouse Gas Control, Vol. 42: pp. 188–199. doi: 10.1016/j.ijggc.2015.07.034.
5. Samsonov, S., Feng, W., Peltier, P., Geirsson, H., d'Oreye, N., and Tiampo, K. 2016. "Multidimensional small baseline subset (MSBAS) for volcano monitoring in two dimensions: Opportunities and challenges. Case study Piton de la Fournaise volcano." Journal of Volcanology and Geothermal Research. doi: 10.1016/j.jvolgeores.2017.04.017.
6. Samsonov, S.V., Lantz, T.C., Kokelj, S.V., and Zhang, Y. 2016. "Growth of a young pingo in the Canadian Arctic observed by RADARSAT-2 interferometric satellite radar." The Cryosphere, Vol. 10(No. 2): pp. 799–810. doi: 10.5194/tc-10-799-2016.
7. Samsonov, S.V., Tiampo, K.F., and Feng, W. 2016. "Fast subsidence in downtown of Seattle observed with satellite radar." Remote Sensing Applications: Society and Environment, Vol. 4: pp. 179–187. doi: 10.1016/j.rsase.2016.10.001.
8. Samsonov S.V. & d'Oreye N. 2017 "Multidimensional Small Baseline Subset (MSBAS) for Two-Dimensional Deformation Analysis: Case Study Mexico City", Canadian Journal of Remote Sensing, 43:4, 318-329, doi: 10.1080/07038992.2017.1344926.